

1 **Probiotic fermentation modifies the structure of pectic polysaccharides from carrot pulp**

2

3 **Yujun Wan<sup>a, b, #</sup>, Tao Hong<sup>a, #</sup>, Huifang Shi<sup>a</sup>, Junyi Yin<sup>a</sup>, Todor Koev<sup>c</sup>, Shaoping Nie<sup>a</sup>,**

4 **Robert G. Gilbert<sup>b, d</sup>, Mingyong Xie<sup>a\*</sup>**

5 <sup>a</sup> *State Key Laboratory of Food Science and Technology, China–Canada Joint Lab of Food*

6 *Science and Technology (Nanchang), Nanchang University, 235 Nanjing East Road,*

7 *Nanchang, Jiangxi 330047, People's Republic of China*

8 <sup>b</sup> *Centre for Nutrition and Food Sciences, Queensland Alliance for Agriculture and Food*

9 *Innovation, The University of Queensland, Brisbane, Queensland, 4072, Australia*

10 <sup>c</sup> *Food, Innovation and Health, Quadram Institute Bioscience, Norwich Research Park,*

11 *Norwich NR4 7UQ, U.K.*

12 <sup>d</sup> *Joint International Research Laboratory of Agriculture and Agri-Product Safety, College of*

13 *Agriculture, Yangzhou University, Yangzhou, Jiangsu 225009, China*

14

15

16 <sup>#</sup> Equal contribution

17 <sup>\*</sup> Corresponding author. [myxie@ncu.edu.cn](mailto:myxie@ncu.edu.cn) (M.Y. Xie)

18 **ABSTRACT:**

19 Polysaccharides from fermented carrot pulp (WSP-p) show better anti-diabetic effects than  
20 those from un-fermented carrot pulp (WSP-n), and functional properties of polysaccharides  
21 depend on their structure. In this study, both WSP-p and WSP-n were separated into three  
22 homogeneous fractions as WSP-p-1, WSP-p-2, WSP-p-3, WSP-n-1, WSP-n-2 and WSP-n-3.  
23 The weight-average molecular weight of all of fractions from WSP-p showed a downward  
24 trend compared with the corresponding fraction from WSP-n. The functional groups in WSP-  
25 p and WSP-n were similar. The morphologies of WSP-p-2 and WSP-p-3 from SEM were  
26 similar to those of WSP-n-2 and WSP-n-3, but there were more fragmented particles adhered  
27 to WSP-n-1 than to WSP-p-1. Monosaccharide composition and methylation analysis  
28 confirmed that WSP-p-1, WSP-p-2, WSP-n-1 and WSP-n-2 were typical rhamnogalacturonan  
29 I-type polysaccharides with 1,4-linked  $\alpha$ -D-galacturonic acid residues, but WSP-p-3 and WSP-  
30 n-3 contained predominantly homogalacturonan regions with 1,4-GalpA linkages.  $^1\text{H}$  and  $^{13}\text{C}$   
31 NMR of fractions from WSP-p showed the similar spectra to those from WSP-n. These  
32 findings suggest that probiotic fermentation mainly cleaved the linkages between repeating  
33 units within polysaccharides during fermentation, and not only reduced their molecular weight  
34 but also improved the homogeneity in their molecular size distribution, which improves their  
35 biofunctions.

36

37 **KEYWORDS:** probiotics fermentation, purification, structure, pectic polysaccharides, carrot

## 38 1. INTRODUCTION

39 Polysaccharides are widely found in plants, animals and microorganisms, and have a range  
40 of biological functions. They have useful bioactivities *in vivo* and *in vitro*, such as functioning  
41 as antidiabetic (Zhao et al., 2018), immune modulation (Baïen et al., 2019) and anticancer  
42 agents (Ying Wang et al., 2020). Their functional activities depend upon their structure. For  
43 example, the triple helical  $\beta$ -glucan from *Lentinus edodes* with lower molecular weight and/or  
44 higher stiffness has stronger antitumor activity than the higher molecular weight and/or lower  
45 stiffness  $\beta$ -glucan from the same source (Zheng, Lu, Xu, & Zhang, 2017), and  $\beta$ -(1,4)-D-  
46 mannans with higher molecular weight (10 MDa) have a higher immunostimulatory activity  
47 than those with lower molecular weight (1.3 MDa) with the same acetylation degree (Ferreira,  
48 Passos, Madureira, Vilanova, & Coimbra, 2015).

49 Probiotic-fermented carrot pulp has been found to have a better anti-diabetic functionality  
50 than the non-fermented pulp, due to more effective regulation of glucose and lipid metabolism  
51 (Li et al., 2014; Li, Nie, Zhu, Xiong, & Xie, 2016). Our previous study showed that the  
52 hypoglycemic effects of both probiotic-fermented and non-fermented carrot pulp arise from its  
53 polysaccharides (Wan, Shi, et al., 2019). Polysaccharides from probiotic fermentation carrot  
54 pulp exhibited more positive effects in ameliorating symptoms in type II diabetic rats, which  
55 is ascribed to changes in structure caused by fermentation. *Lactobacillus plantarum* can modify  
56 polysaccharide structure by degrading glycans to tri- and tetra-saccharides during fermentation  
57 (Kaplan & Hutkins, 2000). Probiotics also use polysaccharides as prebiotics for growth during  
58 this process. However, these effects strongly depend on the linkage structure of these  
59 polysaccharides (Sims, Ryan, & Kim, 2014).

60 The aim of the present study is to compare the fine structure of water-soluble  
61 polysaccharides from probiotic-fermented and non-fermented carrot. To characterize the  
62 structures of complex polysaccharides, the first step is to purify the polysaccharides to obtain

63 several homogeneous fractions. Then, size exclusion chromatography equipped with multi-  
64 angle laser light scattering and differential refractive index detectors is employed to measure  
65 molecular size and weight distributions. Monosaccharide compositions are determined by  
66 high-performance anion-exchange chromatography, and information of functional groups is  
67 obtained using Fourier transform infrared spectroscopy. The morphology of the purified  
68 fractions is imaged with scanning electron microscopy. The position of linkages between  
69 monosaccharide residues is evaluated using methylation analysis. Other details are  
70 characterized with liquid-state proton NMR. The combination of the results could supply the  
71 structural basis for elucidating functional differences.

72

## 73 **2. MATERIALS AND METHODS**

### 74 **2.1 Materials**

75 Probiotics fermented carrot pulp (PFCP) and non-fermented carrot pulp (NFCP) were from  
76 Kuangda Biotech Co. (Nanchang, China) following the process reported elsewhere (Wan, Shi,  
77 et al., 2019). Dextran standards (T-10, T-50, T-80, T-150, T-500 and T-2000), monosaccharide  
78 standards (*L*-fucose (Fuc), *L*-rhamnose (Rha), *D*-arabinose (Ara), *D*-galactose (Gal), *D*-glucose  
79 (Glu), *D*-xylose (Xyl), *D*-mannose (Man), *D*-fructose (Fru), *D*-glucuronic acid (GlcA), and *D*-  
80 galacturonic acid (GalA)), sodium borodeuteride (NaBD<sub>4</sub>) and deuterium oxide (D<sub>2</sub>O) were  
81 purchased from Sigma-Aldrich Co. (St. Louis, USA). All of other reagents were of analytical  
82 grade and were used without further purification.

### 83 **2.2 Preparation of polysaccharides**

84 Water-soluble polysaccharides from PFCP and NFCP, isolated using the same extraction  
85 methods published elsewhere (Wan, Shi, et al., 2019), are denoted WSP-p and WSP-n  
86 respectively. Briefly, either NFCP or PFCP was extracted with deionized water twice at 100 °C  
87 for 2 h. The polysaccharide in the extracting solution was precipitated using ethanol at 4 °C

88 overnight after concentrating to half the original volume under reduced pressure. The  
89 precipitate was then redissolved in deionized water and treated with chloroform and N-butanol  
90 to remove the protein, based on the Sevag method (Staub, 1965). Finally, the liquid was  
91 dialyzed, concentrated and lyophilized to produce WSP-p and WSP-n.

## 92 **2.3 Purification of WSP-p and WSP-n**

93 An ÄKTA Purifier system (GE Healthcare Bio-sciences, USA) equipped with a HiLoad  
94 26/60 Superdex-200 column was employed to purify the polysaccharide, and the eluent was  
95 divided into three fractions for both WSP-p and WSP-n (Wan, Shi, et al., 2019). A 500 mg  
96 sample of WSP-p or WSP-n was dissolved in distilled water containing 0.02% (w/w) NaN<sub>3</sub>  
97 and eluted with 0.1 M NaCl at a flow rate of 1.5 mL/min at 25 °C in the purifier system. These  
98 fractions of the eluant were collected, monitoring with the refractive index detector (RID). The  
99 elution profiles of both WSP-n and WSP-p recorded by the RID showed three overlapping  
100 elution peaks, denoted WSP-n-1, WSP-n-2, WSP-n-3, and WSP-p-1, WSP-p-2 and WSP-p-3.

## 101 **2.4 Characterization of purified fractions**

### 102 2.4.1 Size exclusion chromatography (SEC)

103 The molecular size distributions (MSDs) and weight-average molecular weights  $\bar{M}_w$  of six  
104 purified fractions were obtained from the SEC data as described elsewhere (Watts, Gray-Weale,  
105 & Gilbert, 2007), using a SEC system equipped with an Ohpak SB-G guard column (50 mm ×  
106 6.0 mm I.D., 10 μm), an SB-806 HQ column (300 mm × 8.0 mm I.D., 13 μm) and an SB-804  
107 HQ column (300 mm × 8.0 mm I.D., 10 μm) (Shodex Denko America, USA) in series, a  
108 refractive index detector (Wyatt, USA) and a multiple-angle laser light scattering detector  
109 (MALLS) (Wyatt, USA), following the procedure described elsewhere (Wan, Xu, et al., 2019).  
110 A 100 μL sample was injected into the MALLS-SEC system and eluted with the mobile phase  
111 (0.02% (w/w) NaN<sub>3</sub> and 0.1 M NaNO<sub>3</sub>) at 35 °C with a flow rate of 0.6 mL/min.

### 112 2.4.2 Monosaccharide compositions

113 These purified fractions were hydrolyzed in an oil bath with 2 M H<sub>2</sub>SO<sub>4</sub> at 100 °C for 4 h  
114 and then diluted by adding distilled water, before injecting into the high-performance anion  
115 exchange chromatography device (Thermo Fisher, USA) to analyze their monosaccharide  
116 compositions. The detailed separation procedure was the same as in our previous report (Wu,  
117 Liu, Wan, Huang, & Nie, 2019).

#### 118 2.4.3 Fourier transform infrared (FTIR) spectroscopy

119 1 mg of dried purified fraction was ground with 100 mg KBr powder and pressed into pellets  
120 to analyze the functional groups using a Fourier transform infrared spectrophotometer (Thermo  
121 Fisher, USA) over the frequency range 400 to 4,000 cm<sup>-1</sup>.

#### 122 2.4.4 Scanning electron microscopy

123 All purified fractions were dissolved in deionized water to a final concentration of 1 mg/mL  
124 and then freeze-dried to obtain the dried samples. The morphology of these samples was  
125 characterized by scanning electron microscopy (SEM, JEOL, Japan) at room temperature under  
126 an acceleration voltage of 5 kV.

#### 127 2.4.5 Methylation and GC-MS analysis

128 A slightly modified methylation method was used based on that of (Nie et al., 2011) was  
129 used to analyze the assignments of linkages in these six fractions. Briefly, the dried sample (2-  
130 3 mg) was dissolved in 2 mL of anhydrous dimethyl sulfoxide (DMSO) by sonication for 3 h  
131 and then stirred at 80 °C for 2 h, following by stirring at room temperature overnight to  
132 completely dissolve the sample. 30 mg of dried sodium hydroxide powder was added to the  
133 solution and stirred at room temperature for 3 h. To the mixture was then added 1 mL methyl  
134 iodide and the mixture stirred for another 2.5 h to enable the methylation reaction to take place.  
135 A few drops of deionized water were added to terminate the reaction and the methylated sample  
136 was extracted with 3 mL methylene chloride, followed by hydrolysis with trifluoroacetic acid  
137 and acetylation with acetic anhydride, to obtain the partially methylated alditol acetates

138 (PMAAs). The PMAAs were then dissolved in methylene chloride and injected into an Agilent  
139 7890B/7000D system equipped with a SP-2330 column (Agilent, USA). The system  
140 temperature program was increased from 160 °C to 210 °C at 2 °C/min and then to 240 °C at  
141 5 °C/min (Wang, Yin, Huang, & Nie, 2020).

#### 142 2.4.6 Nuclear magnetic resonance (NMR) spectroscopy

143 The six fractions were dissolved in D<sub>2</sub>O, then lyophilized using a freezer dryer; this was  
144 repeated three times to completely remove the exchanged protons. After that, these samples  
145 were dissolved in D<sub>2</sub>O at room temperature to conduct the NMR experiments. The <sup>1</sup>H spectra  
146 and <sup>13</sup>C spectra were obtained at 313 K with a Bruker Avance 600 MHz NMR spectrometer  
147 (Bruker, Germany).

148 <sup>1</sup>H spectra were obtained using the integrated zg30 pulse program, with a 30° flip angle of 10.0  
149 μs and recycle delay of 1.0 s, 64 scans and 2 dummy scans, whereas <sup>13</sup>C spectra were obtained  
150 using the zgpg30 pulse program with 30° flip angle of 10.0 s, recycle delay of 2.0 s and cpd2  
151 decoupling sequence, 65000 scans and 4 dummy scans. <sup>1</sup>H-<sup>1</sup>H nuclear Overhauser effect  
152 spectroscopy (nOeSY) experiments were performed using the noesygpqh pulse sequence,  
153 where the acquisition parameters were 90° flip angle of 10.0 μs, gradient pulses of 0.2 ms,  
154 mixing time of 0.3 s, recycle delay of 2 s, 32 scans and 32 dummy scans. <sup>1</sup>H-<sup>1</sup>H correlation  
155 spectroscopy (COSY) experiments were performed using the cosygpmfqp pulse sequence, with  
156 acquisition parameters of 90° flip angle of 10.0 μs, gradient pulse of 1000 μs, incremental delay  
157 of 3.0 μs, gradient recovery delay of 0.2 ms, recycle delay of 2.0 s, 128 scans and 16 dummy  
158 scans. <sup>1</sup>H-<sup>13</sup>C heteronuclear single quantum correlation (HSQC) spectroscopy experiments  
159 were performed using the integrated hsqcetgp pulse sequence, with acquisition parameters of  
160 90° flip angle of 10.0 μs, trim pulse of 1.0 ms, gradient recover delay of 0.2 ms, recycle delay  
161 of 1.5 s, 64 scans and 16 dummy scans. <sup>1</sup>H-<sup>13</sup>C heteronuclear multiple bond correlation (HMBC)  
162 spectroscopy experiments were obtained using the hmbcgpndqf pulse sequence, with

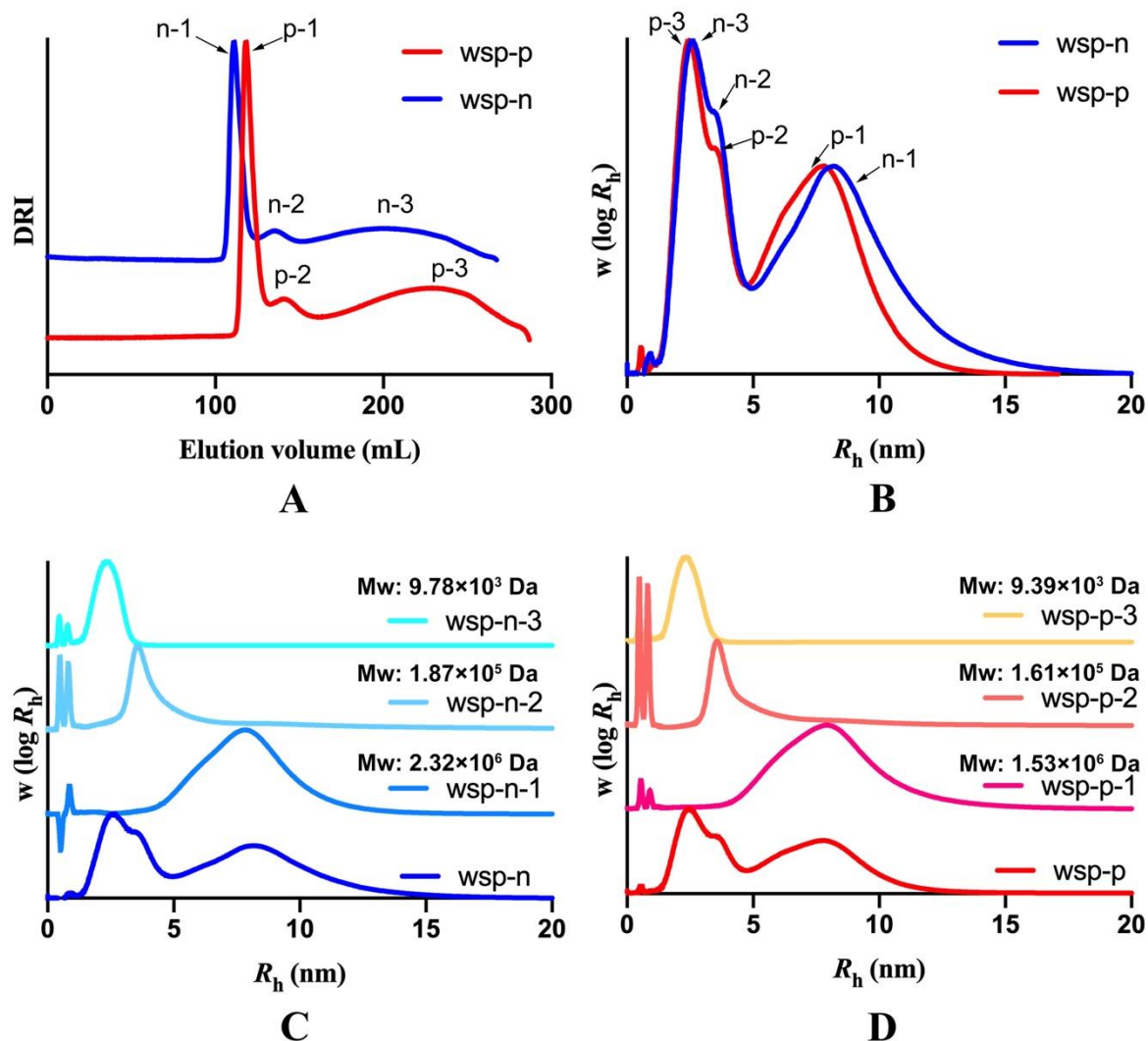
163 acquisition parameters of  $^{13}\text{C}$  90° flip angle of 10.0  $\mu\text{s}$ ,  $^{13}\text{C}$  180° flip angle of 20.0  $\mu\text{s}$ ,  $^1\text{H}$  90°  
164 flip angle of 10.0  $\mu\text{s}$ , gradient pulse of 1.0 ms, gradient recovery delay of 0.2 ms, recycle delay  
165 of 1.5 s, 128 scans and 16 dummy scans.

166

### 167 **3. Results and discussion**

168 SEC elution curves (Fig. 1A) from the ÄKTA Purifier system showed that both WSP-n and  
169 WSP-p were triplets, denoted WSP-n-1, WSP-n-2, WSP-n-3, WSP-p-1, WSP-p-2 and WSP-p-  
170 3, respectively. The yield of these six fractions was 15.20% (WSP-n-1), 5.16% (WSP-n-2),  
171 16.58% (WSP-n-3), 13.42% (WSP-p-1), 2.50% (WSP-p-2) and 19.10% (WSP-p-3). The data  
172 from SEC (Fig. 1B) also confirmed that there were three components in the molecular size  
173 from the SEC results (Fig. 1C and 1D), since there was only one molecular size distribution to  
174 each fraction. The SEC results also showed that the  $\bar{M}_w$  for each fraction from WSP-p was  
175 lower than the corresponding fractions in WSP-n, and this implied that probiotics used these  
176 polysaccharides to promote the growth since these polysaccharides could serve as potential  
177 prebiotics (P. Chen et al., 2019).





178

179 **Figure 1.** Elution curves and molecular size distributions (MSDs) (A. Elution curves of wsp-p and wsp-n; B.  
 180 MSDs of wsp-p and wsp-n; C. MSDs of wsp-n-1, wsp-n-2 and wsp-n-3; D. MSDs of wsp-p-1, wsp-p-2 and wsp-  
 181 p-3)

### 182 3.2 Monosaccharide compositions

183 Table 1 shows that all six purified fractions were typical pectic polysaccharides, mainly  
 184 containing Rha, Ara, Gal and GalA as their monomer units. Glucose may originate from the  
 185 non-pectic polysaccharides, such as cellulose and hemicellulose (Deng et al., 2020). Neutral  
 186 sugars predominated in WSP-n-1, WSP-n-2, WSP-p-1 and WSP-p-2 (> 85% in all four  
 187 fractions). By contrast, there were more than 70% uronic acid units within both WSP-n-3 and  
 188 WSP-p-3. GalA is the main monomer unit of homogalacturonan (HG) and rhamnogalacturonan  
 189 (RG) (Deng et al., 2020). Table 1 shows that all of these six fractions had the RG and HG

190 domain within their structure. The molar components of the RG-I and HG domains have been  
 191 estimated as follows:  $RG-I = (GalA - HG) + Rha + Ara + Gal$ ,  $HG = GalA - Rha$  (E. G.  
 192 Shakhmatov, Toukach, Michailowa, & Makarova, 2014). RG-I was the predominant  
 193 component in both fractions 1 and 2. The HG domains within WSP-n-1 and WSP-n-2  
 194 decreased after fermentation, but their RG-I domains increased. HG was the main constituent  
 195 within fraction 3, being higher than 60% in both of WSP-n-2 and WSP-p-2.

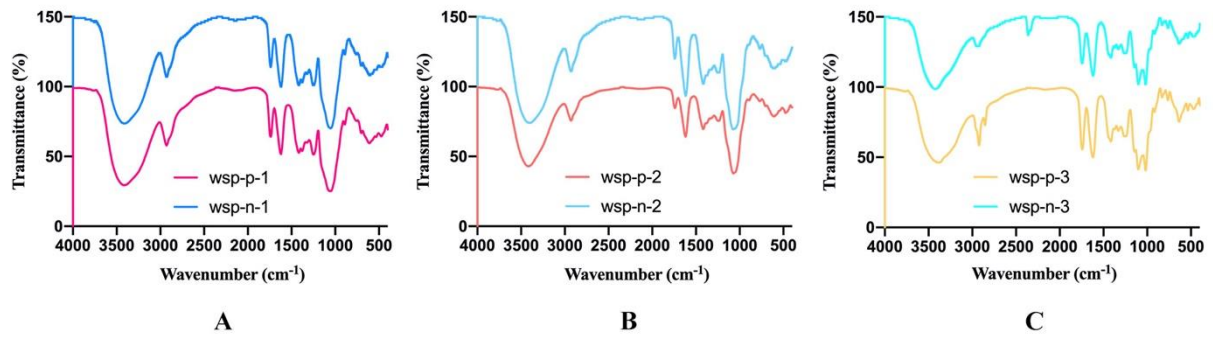
196 **Table 1.** Chemical compositions of purified fractions <sup>α</sup>

	<b>Rha (%)</b>	<b>Ara (%)</b>	<b>Gal (%)</b>	<b>Glc (%)</b>	<b>GalA (%)</b>
<b>WSP-n-1</b>	6.45 ± 1.05 <sup>a</sup>	32.87 ± 1.11 <sup>a</sup>	49.01 ± 1.23 <sup>a</sup>	1.12 ± 0.07 <sup>a</sup>	10.55 ± 0.89 <sup>a</sup>
<b>WSP-p-1</b>	8.80 ± 0.61 <sup>b</sup>	30.75 ± 0.64 <sup>a</sup>	47.68 ± 1.54 <sup>a</sup>	0.95 ± 0.06 <sup>a</sup>	11.82 ± 0.10 <sup>a</sup>
<b>WSP-n-2</b>	4.57 ± 0.27 <sup>a</sup>	33.85 ± 0.32 <sup>a</sup>	45.93 ± 0.40 <sup>a</sup>	3.30 ± 0.79 <sup>a</sup>	12.30 ± 1.20 <sup>a</sup>
<b>WSP-p-2</b>	5.88 ± 0.23 <sup>a</sup>	35.05 ± 0.75 <sup>b</sup>	46.26 ± 0.60 <sup>b</sup>	1.06 ± 0.05 <sup>a</sup>	11.75 ± 0.65 <sup>a</sup>
<b>WSP-n-3</b>	5.39 ± 0.03 <sup>a</sup>	7.61 ± 0.02 <sup>a</sup>	7.70 ± 0.04 <sup>a</sup>	8.82 ± 0.24 <sup>a</sup>	70.53 ± 0.16 <sup>a</sup>
<b>WSP-p-3</b>	4.72 ± 0.06 <sup>a</sup>	9.55 ± 0.05 <sup>b</sup>	9.55 ± 0.02 <sup>b</sup>	3.23 ± 0.06 <sup>b</sup>	73.98 ± 0.76 <sup>b</sup>

197 <sup>α</sup> Different letters represent significant differences ( $p < 0.05$ )

### 198 3.3 FTIR

199 Fig. 2 shows the FTIR spectra of the six purified fractions. An absorption at around 3400  
 200  $cm^{-1}$  is attributed to the hydroxyl group, the band at approximately 2930  $cm^{-1}$  to a C-H stretch,  
 201 that at about 1640  $cm^{-1}$  to a carboxylate group near 1750  $cm^{-1}$  to esterified carboxyl groups;  
 202 this last also overlaps with the free carboxyl group. It is seen that each of the purified fractions  
 203 (WSP-n-1, WSP-n-2 and WSP-n-3) contains the same functional groups as the corresponding  
 204 fractions in WSP-p. This result indicated that probiotics fermentation did not change the  
 205 functional group of polysaccharides from carrot.

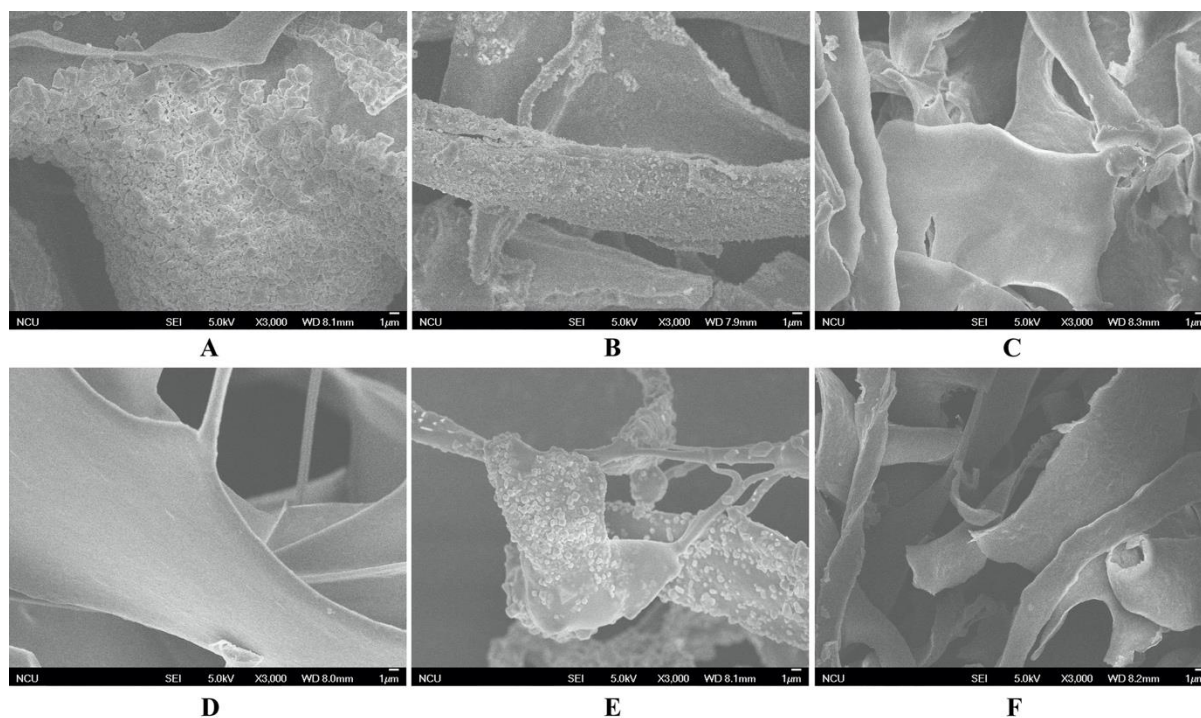


206

207 **Figure 2.** FTIR spectra of purified fractions

208 3.4 SEM

209 Fig. 3 compares the SEM micrographs of these six different purified fractions. All of these  
 210 samples had multi-layer arrangements and showed highly inter-connected networks. There was  
 211 an obvious difference between WSP-n-1 and WSP-p-1. While the morphology of WSP-n-1  
 212 showed many fragmented particles adhering to large particles, that of WSP-p-1 only had large  
 213 particles with smooth surfaces. Both images of WSP-n-2 and WSP-p-2 showed similar rough  
 214 surfaces, but WSP-n-3 and WSP-p-3 had smoother surfaces. These results suggest that there  
 215 still were some minor changes in their structural features, since the morphologies of WSP-p-1  
 216 and WSP-n-1 showed some differences, and the morphology difference represented the  
 217 difference in their structure (Qi et al., 2020).



218

219 **Figure 3.** SEM micrographs of different purified fractions (A. WSP-n-1, B. S WSP-n-2, C. WSP-n-3, D. WSP-  
 220 p-1, E. WSP-p-2 and F. WSP-p-3)

### 221 3.5 Linkages pattern

222 Results from methylation analysis of the reduced WSP-n-1 and WSP-p-1 are shown in Table  
 223 2. The fermentation process did not noticeably change the linkage patterns of fraction 1 purified  
 224 from carrot polysaccharide because the glycosidic bonds types of WSP-n-1 and WSP-p-1  
 225 remained basically the same. Results from the GC-MS showed that the glycosidic bonds types  
 226 of these two polysaccharides were similar. However, there are some differences in the molar  
 227 ratio of their glycosidic bonds. The structure of fraction 1 (both WSP-n-1 and WSP-p-1) was  
 228 complex, with nearly 20 types of linkage patterns, in which 1,4-Galp, 1,5-Araf and T-Araf  
 229 residues were the main residues. Additionally, the presence of 1,2,4-Rhap, 1,3,5-Araf, T-Galp,  
 230 1,4-GalpA and 1,4,6-Galp residues were detected. The results of linkage pattern analysis of  
 231 WSP-n-1 and WSP-p-1 indicated that fraction 1 was a typical RG-I type pectin, which is was  
 232 consistent with the results of monosaccharide composition analysis (Atmodjo, Hao, & Mohnen,  
 233 2013; Cardoso, Ferreira, Mafra, Silva, & Coimbra, 2007). The main glycosidic linkage types

234 in WSP-n-2 and WSP-p-2 were similar to fraction 1, including T-Araf, 1,5-Araf and 1,4-Galp  
235 residues (Table 2). Because of the relatively small amount of sample, fraction 2 had to be  
236 subjected to methylation analysis without reduction; thus, information on uronic acid could not  
237 be obtained, and the presence of rhamnose could not be detected (Pettolino, Walsh, Fincher, &  
238 Bacic, 2012).

239 As shown in Table 2, the dominant sugar residue in WSP-n-3 and WSP-p-3 was 1,4-  
240 GalpA, accounting for more than 60 mol% of all the sugar residues, which is in accordance  
241 with the result of monosaccharide composition analysis, that fraction 3 is mainly composed of  
242 GalA. This indicated that WSP-n-3 and WSP-p-3 were typical HG-type pectic polysaccharides  
243 (Evgeny G Shakhmatov, Toukach, & Makarova, 2020), and there were no changes in linkage  
244 pattern of these fractions, and only minor difference in their molar ratio of each linkage pattern.  
245

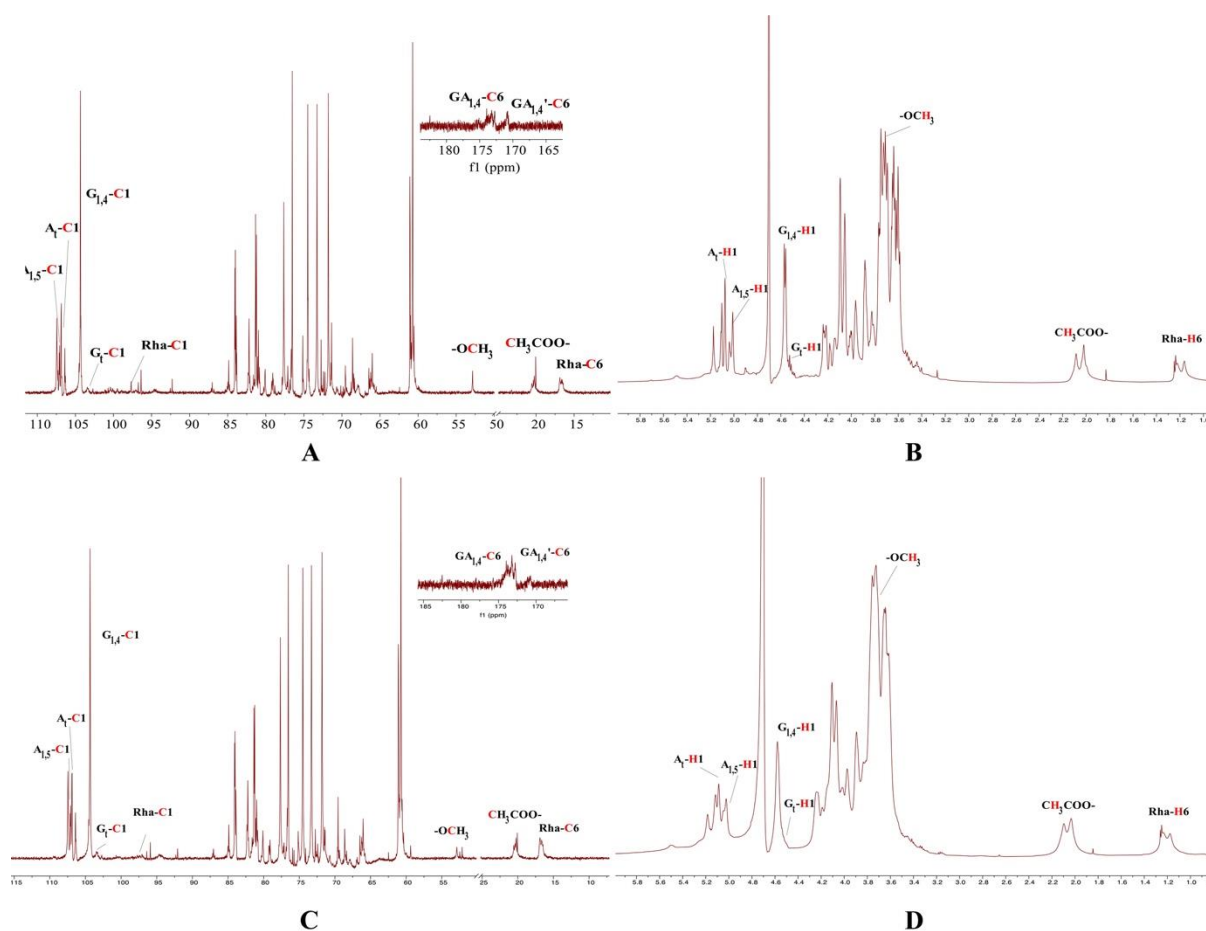
Linkage pattern	WSP-n-1	WSP-p-1	WSP-n-2	WSP-p-2	WSP-n-3	WSP-p-3
T-Araf	16.63	14.28	31.94	31.68	2.19	4.68
1,2-Rhap	2.15	3.27	n.d.	n.d.	n.d.	n.d.
T-Galp	5.02	5.90	2.95	2.67	8.59	11.90
1,5-Araf	11.59	12.56	20.71	20.44	4.64	2.65
1,2,4-Rhap	6.06	7.16	n.d.	n.d.	n.d.	n.d.
1,3,5-Araf	5.8	6.38	9.14	5.99	n.d.	n.d.
1,4-Galp	29.32	24.64	22.74	17.78	1.39	1.52
1,4-GalAp	7.45	6.32	n.d.	n.d.	67.01	61.24
1,2,5-Araf	2.48	2.76	4.12	3.14	n.d.	n.d.
1,4-Glcp	0.65	1.32	n.d.	n.d.	3.01	2.19
1,6-Galp	1.03	1.31	1.99	6.46	1.48	2.51
1,3,4-Galp	1.7	2.09	n.d.	n.d.	3.02	3.32
1,2,4-Galp	2.67	2.69	n.d.	n.d.	2.01	2.19
1,2,3,4-Galp	0.60	0.79	n.d.	n.d.	n.d.	n.d.
1,4,6-Galp	4.76	6.00	1.98	1.02	5.86	6.64
1,3,6-Galp	0.37	0.50	2.74	8.78	0.78	1.15
1,3,4,6-Galp	0.76	1.08	1.69	2.06	n.d.	n.d.
1,2,4,6-Galp	0.94	0.96	n.d.	n.d.	n.d.	n.d.

247 <sup>a</sup> n.d.: Not detected

## 248 3.6 NMR

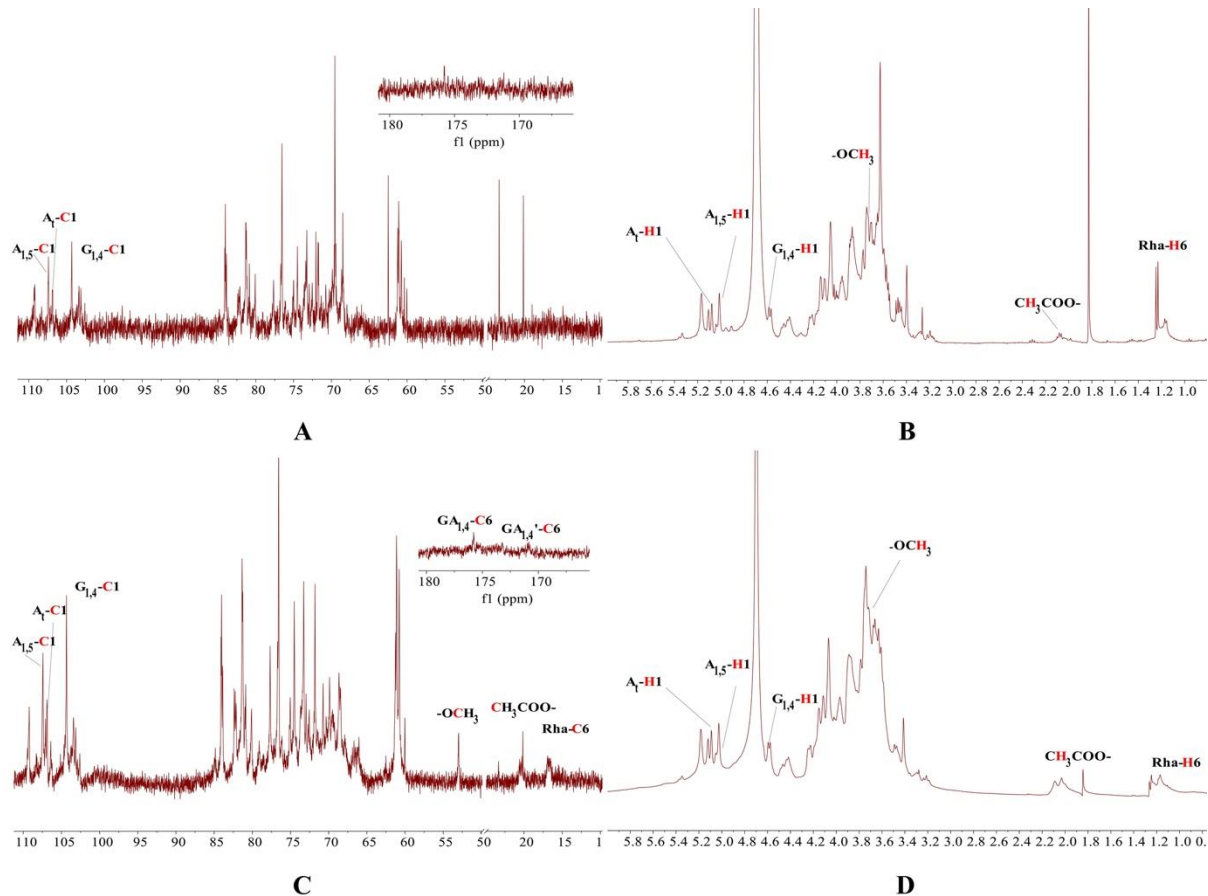
249 The <sup>13</sup>C and <sup>1</sup>H spectra of WSP-n-1 and WSP-p-1 are presented in Figure 4. From the  
250 similarity of the NMR spectra, it seems that the fermentation process did not significantly  
251 change the structural features of fraction 1. In accordance with the complex methylation  
252 analysis results, the anomeric proton and carbon region of WSP-n-1 and WSP-p-1 were  
253 relatively complicated. This was in accordance with all 2D NMR spectra, where the difference  
254 in chemical shift and cross-peak position varied minimally between WSP-n-1 and WSP-p-1  
255 fractions. The resonances at  $\delta$  4.54/104.08 ppm and 4.56/103.41 ppm corresponded to the

256 anomeric proton and carbon of  $\beta$ -1,4-Galp and  $\beta$ -T-Galp, respectively. For arabinose residues,  
 257 signals at  $\delta$  5.06/106.66 ppm and 5.00/107.08 ppm are assigned to  $\alpha$ -T-Araf and  $\alpha$ -1,5- Araf  
 258 (Dias, Barbieri, Fetzer, Corazza, & Silveira, 2020; Rakhmanberdyeva, Zhauynbayeva,  
 259 Senchenkova, Shashkov, & Bobakulov, 2019). The small peaks at high field,  $\delta$  1.22 ppm in the  
 260  $^1\text{H}$  spectrum and 16.54 ppm in the  $^{13}\text{C}$  spectrum, are assigned to the  $\text{CH}_3$  (C6) of rhamnose,  
 261 demonstrating the presence of this sugar residue. The anomeric proton and carbon of rhamnose  
 262 are assigned to  $\delta$  4.89/97.67 ppm. The signals present at low field,  $\delta$  175–170 ppm, in the  $^{13}\text{C}$   
 263 spectrum are assigned to the carboxyl carbons of GalpA, indicating the presence of uronic acid  
 264 and methyl-esterified uronic acid, which is consistent with the monosaccharide composition  
 265 results (Patova et al., 2019).



266  
 267 **Figure 4.**  $^{13}\text{C}$  NMR spectra of WSP-n-1 (a) and WSP-p-1 (c);  $^1\text{H}$  NMR of WSP-n-1 (b) and WSP-p-1 (d). GA:  
 268 GalpA.

269 Because of the relatively small amount of sample, the quality of the NMR spectra of WSP-  
 270 n-2 and WSP-p-2 are not ideal. However, the signals of this fraction are similar to those of  
 271 fraction 1, mainly containing peaks of  $\beta$ -1,4-Galp,  $\beta$ -T-Galp,  $\alpha$ -T-Araf and  $\alpha$ -1,5-Araf,  
 272 indicating the compositional similarity of fraction 1 and 2.

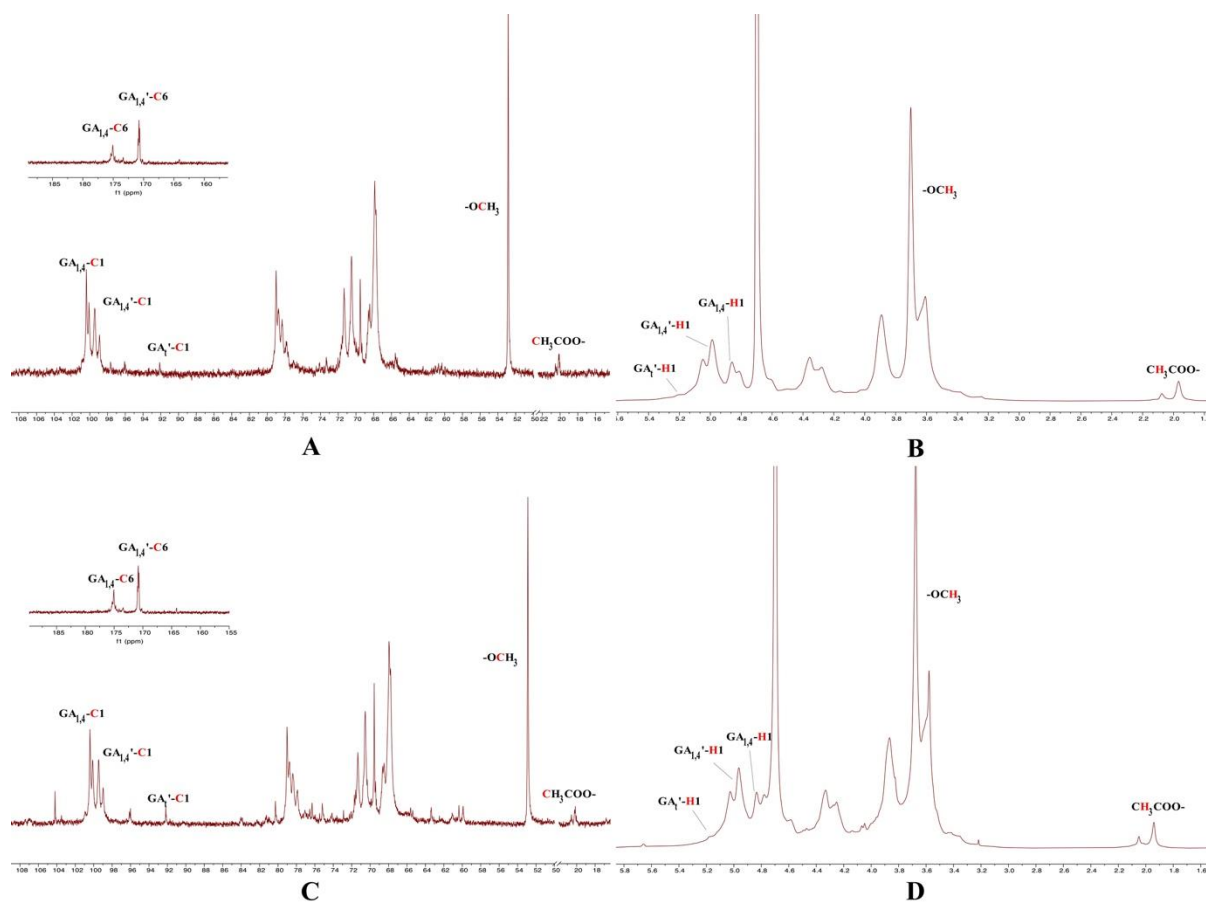


273  
 274 **Figure 5.**  $^{13}\text{C}$  NMR of WSP-n-2 (a) and WSP-p-2 (c);  $^1\text{H}$  NMR of WSP-n-2 (b) and WSP-p-2 (d). GA: GalpA;  
 275 GA': GalpA(OMe) ; G: Galp; A: Ara.

276 The results also suggest that the probiotic fermentation process had only minor influence  
 277 on the structure of carrot water-soluble polysaccharide fraction 3, where no differences were  
 278 detected in the 2D spectra of the unfermented and fermented fractions. Fraction 3 was a typical  
 279 HG-type polysaccharide, as confirmed by the NMR results. Signals at  $\delta$  4.87 ppm, 5.01 ppm  
 280 and 5.22 ppm in the  $^1\text{H}$  spectrum and  $\delta$  99.94 ppm, 99.16 ppm and 92.13 ppm in the  $^{13}\text{C}$   
 281 spectrum are assigned to anomeric proton and carbon signals of  $\alpha$ -1,4-GalpA, methyl esterified  
 282  $\alpha$ -1,4-GalpA (GalpAme) and  $\alpha$ -T-GalpA residues, respectively. The signals at  $\delta$  175.53 ppm



283 and 170.87 ppm in the  $^{13}\text{C}$  spectrum were assigned to C6 of  $\alpha$ -1,4-GalpA and methyl esterified  
 284  $\alpha$ -1,4-GalpA (Patova et al., 2019). The most intense and sharpest peak at  $\delta$  3.72 ppm in the  $^1\text{H}$   
 285 spectrum and  $\delta$  52.82 ppm in the  $^{13}\text{C}$  spectrum in Fig. 4 is attributed to the methoxy group,  
 286 indicating some of the carboxyl groups of  $\alpha$ -1,4-GalpA residues were methyl esterified (Guo,  
 287 Du, Jiang, Goff, & Cui, 2019). Additionally, signals at  $\delta$  2.08 ppm in the  $^1\text{H}$  spectrum and  $\delta$   
 288 20.16 ppm in the  $^{13}\text{C}$  spectrum was assigned to acetyl groups, suggesting O-acetate substitution  
 289 in  $\alpha$ -1,4-GalpA residues (Patova et al., 2019).



290  
 291 **Figure 6.**  $^{13}\text{C}$  NMR of WSP-n-3 (a) and WSP-p-3 (c);  $^1\text{H}$  NMR of WSP-n-3 (b) and WSP-p-3 (d). GA: GalpA;  
 292 GA': GalpA(OMe)

293

#### 294 4. Conclusions

295 The structural comparison studies of these six pectic polysaccharides provide show the  
 296 effects of probiotics fermentation on structural changes of carrot polysaccharides. WSP-n-1,

297 WSP-n-2, WSP-p-1 and WSP-p-2 are typical RG-I pectic polysaccharides with similar  
298 structural features. However, WSP-n-3 and WSP-p-3 are predominantly HG-type pectic  
299 polysaccharides. The probiotics seem to only cleave the linkages between repeating units  
300 within these polysaccharides and then use the products to support to their growth during  
301 fermentation process (P. Chen et al., 2019). Thus, the molecular weights of these three fractions  
302 from WSP-p are lower than those from WSP-n. At the same time, because of the modification  
303 by probiotic fermentation, the purified fractions from WSP-p showed the more homogeneous  
304 molecular size distributions than the corresponding fractions from WSP-n. Since they have the  
305 same repeating units, their linkage pattern and NMR spectra show similar features. All these  
306 characterization results from these six fractions suggest that the differences in functional  
307 activities between WSP-n and WSP-p arise from differences in their fine structural features.  
308 The modified WSP (WSP-p) was the polysaccharides with the lower molecular weight and  
309 more homogeneous glycan than the original WSP (WSP). These modified polysaccharides  
310 probably have higher scavenging rates for reactive oxygen species and then may help to protect  
311 cells against impairments to blood-sugar regulation (X. Q. Chen et al., 2011; Xiao & Jiang,  
312 2015). However, it is also should be noted that techniques to characterize the complex pectic  
313 polysaccharides are immature, since the substrates in the present study contain mainly GalA as  
314 their monomer unit. Therefore, there may be more difference between WSP-n and WSP-p,  
315 which is an area for further investigation.

316

### 317 **Acknowledgement**

318 This work was supported from the National Natural Science Foundation of China  
319 (31571826), the Outstanding Science and Technology Innovation Team Project in Jiangxi  
320 Province (20165BCB19001), and the Collaborative Project in Agriculture and Food Field  
321 between China and Canada (2017ZJGH0102001).

323 **References**

- 324 Atmodjo, M. A., Hao, Z., & Mohnen, D. (2013). Evolving views of pectin biosynthesis. *Annual*  
 325 *Review Plant Biology*, 64, 747-779.
- 326 Baien, S. H., Seele, J., Henneck, T., Freibrodt, C., Szura, G., Moubasher, H., . . . Singh, M.  
 327 (2019). Antimicrobial and immunomodulatory effect of Gum arabic on human and  
 328 bovine granulocytes against *Staphylococcus aureus* and *Escherichia coli*. *Frontiers in*  
 329 *Immunology*, 10, 3119.
- 330 Cardoso, S. M., Ferreira, J. A., Mafra, I., Silva, A. M., & Coimbra, M. A. (2007). Structural  
 331 ripening-related changes of the arabinan-rich pectic polysaccharides from olive pulp  
 332 cell walls. *Journal of Agricultural and Food Chemistry*, 55(17), 7124-7130.
- 333 Chen, P., You, Q., Li, X., Chang, Q., Zhang, Y., Zheng, B., . . . Zeng, H. (2019). Polysaccharide  
 334 fractions from *Fortunella margarita* affect proliferation of *Bifidobacterium adolescentis*  
 335 ATCC 15703 and undergo structural changes following fermentation. *International*  
 336 *Journal of Biological Macromolecules*, 123, 1070-1078.
- 337 Chen, X. Q., Wang, Y. F., Wu, Y. L., Han, B. Y., Zhu, Y. J., Tang, X. L., & Sun, Q. L. (2011).  
 338 Green tea polysaccharide-conjugates protect human umbilical vein endothelial cells  
 339 against impairments triggered by high glucose. *International Journal of Biological*  
 340 *Macromolecules*, 49(1), 50-54.
- 341 Deng, Z., Pan, Y., Chen, W., Chen, W., Yun, Y., Zhong, Q., . . . Chen, H. (2020). Effects of  
 342 cultivar and growth region on the structural, emulsifying and rheological characteristic  
 343 of mango peel pectin. *Food Hydrocolloids*, 103, 105707.
- 344 Dias, I. P., Barbieri, S. F., Fetzer, D. E. L., Corazza, M. L., & Silveira, J. L. M. (2020). Effects  
 345 of pressurized hot water extraction on the yield and chemical characterization of pectins  
 346 from *Campomanesia xanthocarpa* Berg fruits. *International Journal of Biological*  
 347 *Macromolecules*, 146, 431-443.
- 348 Ferreira, S. S., Passos, C. P., Madureira, P., Vilanova, M., & Coimbra, M. A. (2015). Structure–  
 349 function relationships of immunostimulatory polysaccharides: A review. *Carbohydrate*  
 350 *Polymers*, 132, 378-396.
- 351 Guo, Q., Du, J., Jiang, Y., Goff, H. D., & Cui, S. W. (2019). Pectic polysaccharides from  
 352 hawthorn: Physicochemical and partial structural characterization. *Food Hydrocolloids*,  
 353 90, 146-153.
- 354 Kaplan, H., & Hutkins, R. W. (2000). Fermentation of fructooligosaccharides by lactic acid  
 355 bacteria and bifidobacteria. *Applied and Environmental Microbiology*, 66(6), 2682-  
 356 2684.
- 357 Li, C., Ding, Q., Nie, S., Zhang, Y., Xiong, T., & Xie, M. (2014). Carrot juice fermented with  
 358 *Lactobacillus plantarum* NCU116 ameliorates type 2 diabetes in rats. *Journal of*  
 359 *Agricultural and Food Chemistry*, 62(49), 11884-11891.
- 360 Li, C., Nie, S., Zhu, K., Xiong, T., & Xie, M. (2016). *Lactobacillus plantarum* NCU116  
 361 fermented carrot juice evokes changes of metabolites in serum from type 2 diabetic rats.  
 362 *Food Research International*, 80, 36-40.
- 363 Nie, S., Cui, S. W., Phillips, A. O., Xie, M., Phillips, G. O., Al-Assaf, S., & Zhang, X. (2011).  
 364 Elucidation of the structure of a bioactive hydrophilic polysaccharide from *Cordyceps*  
 365 *sinensis* by methylation analysis and NMR spectroscopy. *Carbohydrate Polymers*,  
 366 84(3), 894-899.
- 367 Patova, O., Smirnov, V., Golovchenko, V., Vityazev, F., Shashkov, A., & Popov, S. (2019).  
 368 Structural, rheological and antioxidant properties of pectins from *Equisetum arvense* L.  
 369 and *Equisetum sylvaticum* L. *Carbohydrate Polymers*, 209, 239-249.

370 Pettolino, F. A., Walsh, C., Fincher, G. B., & Bacic, A. (2012). Determining the polysaccharide  
371 composition of plant cell walls. *Nature Protocol*, 7(9), 1590-1607.

372 Qi, X. L., Su, T., Zhang, M. Y., Tong, X. Q., Pan, W. H., Zeng, Q. K., & Shen, J. L. (2020).  
373 Sustainable, flexible and biocompatible hydrogels derived from microbial  
374 polysaccharides with tailorable structures for tissue engineering. *Carbohydrate*  
375 *Polymers*, 237, 116160.

376 Rakhmanberdyeva, R., Zhaunbayeva, K., Senchenkova, S., Shashkov, A., & Bobakulov, K.  
377 M. (2019). Structure of arabinogalactan and pectin from the *Silybum marianum*.  
378 *Carbohydrate Research*, 485, 107797.

379 Shakhmatov, E. G., Toukach, P. V., & Makarova, E. N. (2020). Structural studies of the pectic  
380 polysaccharide from fruits of *Punica granatum*. *Carbohydrate Polymers*, 235, 115978.

381 Shakhmatov, E. G., Toukach, P. V., Michailowa, C., & Makarova, E. N. (2014). Structural  
382 studies of arabinan-rich pectic polysaccharides from *Abies sibirica* L. Biological  
383 activity of pectins of *A. sibirica*. *Carbohydrate Polymers*, 113, 515-524.

384 Sims, I. M., Ryan, J. L., & Kim, S. H. (2014). In vitro fermentation of prebiotic  
385 oligosaccharides by *Bifidobacterium lactis* HN019 and *Lactobacillus* spp. *Anaerobe*,  
386 25, 11-17.

387 Staub, A. (1965). Removal of protein-Sevag method. *Methods in Carbohydrate Chemistry*, 5,  
388 5-6.

389 Wan, Y., Shi, H., Xu, R., Yin, J., Nie, S., Xiong, T., & Xie, M. (2019). Origin of Hypoglycemic  
390 Benefits of Probiotic-Fermented Carrot Pulp. *Journal of Agricultural and Food*  
391 *Chemistry*, 67(3), 895-904.

392 Wan, Y., Xu, M., Gilbert, R. G., Yin, J., Huang, X., Xiong, T., & Xie, M. (2019). Colloid  
393 chemistry approach to understand the storage stability of fermented carrot juice. *Food*  
394 *Hydrocolloids*, 89, 623-630.

395 Wang, Y., Han, Q., Bai, F., Luo, Q., Wu, M., Song, G., . . . Wang, Y. (2020). The assembly  
396 and antitumor activity of lycium barbarum polysaccharide-platinum-based conjugates.  
397 *Journal of Inorganic Biochemistry*, 205, 1-10.

398 Wang, Y., Yin, J., Huang, X., & Nie, S. (2020). Structural characteristics and rheological  
399 properties of high viscous glucan from fruit body of *Dictyophora rubrovolvata*. *Food*  
400 *Hydrocolloids*, 101, 1-10.

401 Watts, C. J., Gray-Weale, A., & Gilbert, R. G. (2007). Interpreting size-exclusion data for  
402 highly branched biopolymers by reverse Monte Carlo simulations. *Biomacromolecules*,  
403 8(2), 455-463.

404 Wu, G., Liu, D., Wan, Y., Huang, X., & Nie, S. (2019). Comparison of hypoglycemic effects  
405 of polysaccharides from four legume species. *Food Hydrocolloids*, 90, 299-304.

406 Xiao, J. B., & Jiang, H. X. (2015). A Review on the Structure-Function Relationship Aspect  
407 of Polysaccharides from Tea Materials. *Critical Reviews in Food Science and Nutrition*,  
408 55(7), 930-938.

409 Zhao, L., Zhang, F., Ding, X., Wu, G., Lam, Y. Y., Wang, X., . . . Ma, J. (2018). Gut bacteria  
410 selectively promoted by dietary fibers alleviate type 2 diabetes. *Science*, 359(6380),  
411 1151-1156.

412 Zheng, X., Lu, F., Xu, X., & Zhang, L. (2017). Extended chain conformation of  $\beta$ -glucan and  
413 its effect on antitumor activity. *Journal of Materials Chemistry B*, 5(28), 5623-5631.

414

415